Proceedings of the Twenty-sixth (2016) International Ocean and Polar Engineering Conference **www.isope.org**
Rhodes, Greece, June 26-July 1, 2016

ISBN 978-1-880653-88-3; ISSN 1098-6189

Fully-Coupled Dynamic Response of a Semi-submerged Floating Wind Turbine System in Wind and Waves

Pengfei Li [1], Decheng Wan [1] and Changhong Hu [2]*

1 State Key Laboratory of Ocean Engineering, School of Naval Architecture, Ocean and Civil Engineering, Shanghai Jiao Tong University, Collaborative Innovation Center for Advanced Ship and Deep-Sea Exploration, Shanghai, China
2 Research Institute for Applied Mechanics, Kyushu University, Fukuoka, Japan
* Corresponding author

ABSTRACT

An Unsteady Actuator Line Model (UALM) is developed in this paper and applied to a 5MW floating offshore wind turbine (FOWT). This model is implemented into two- phase fluid CFD solver, naoeFOAM-SJTU. The goal of the approach presented here is to investigate the interaction of the aerodynamic loads with the platform motion within acceptable time cost. A semi-submerged floating platform conceptualized in the Offshore Code Comparison Collaboration (OC4) is considered in this paper. Initially the UALM is verified by comparison with the results of a previous study. Next, two kind of full-system simulations with different complexity are performed: first, the wind forces are simplified into a constant thrust; second, the fully coupled dynamic analysis with wind and wave excitation is conducted by utilizing UALM. Based on the results, the aerodynamic loads and coupled responses for cases of different complexity are discussed.

KEY WORDS: Floating offshore wind turbine, UALM, wind and wave, coupled responses

INTRODUCTION

As with other emerging industries, the wind energy industry moves on with hesitation. According to the statistics of Chinese Wind Energy Association, wind power provided 114.6 GW for China's electricity supply at the end of 2014, which shows a booming trend. The China's offshore wind power is also developing in the fast lane and up to 229.3MW have been installed. Meanwhile, many European countries have begun to move forward towards the floating offshore wind conversion technology. Among the various floating solutions suggested, the most promising are the spar buoy, the tension-leg platform (TLP) and the semi-submersible. The present study, specially focus on a semi-submersible design. A review of current floating supporting strategies is available in Vir´e (2012).

Offshore wind power has many advantages over land-based wind turbines, including large continuous areas suitable for farm deployment, stronger and more steady wind, and less wind turbulence (Musial et al, 2004). However, designing offshore wind turbine system is a challenging task. This is especially true for the floating offshore wind turbine (FOWT).because of the complex coupling effects. This coupling effects are prescribed by Sebastian and Lackner (2013). The additional Degrees of Freedom (DOFs) of the floater result in the highly unsteady properties of aerodynamics of FOWTs. Moreover, significant pitch and surge motion of the floater have been predicted in previous studies (Matha et al, 2011). Therefore, accurate simulation of the coupled dynamics of the FOWT is a substantial task, considering also the existence of very limited large-scale experimental data. The absence of acknowledged software package simulating the full system is also a restricting factor for the development of offshore wind technology. With this in mind, Task 30 OC4 is led cooperatively by the National Renewable Energy Laboratory (NREL) and the Fraunhofer Institute for Wind Energy and Energy Systems Technology (IWES). The purpose of the OC4 project is to perform a benchmarking exercise of offshore wind turbine dynamics computer codes. The project defines the load cases to be run for Phase II and the output to be reported.

Almost all of the design codes currently capable of performing integrated modeling of floating wind turbines (Cordle et al. (2011)) use the Blade Element Momentum (BEM) theory to calculate the aerodynamic forces on rotors. Ramachandran et al. (2013) performed fully coupled dynamic analysis of a TLP FOWT in wave and wind using HAWC2. A simplified analysis of a spar buoy floating wind turbine is presented by Karimirad & Moan (2012). The coupled Simo-Riflex-TDHMILL codes were used in this study. The Panel method and the Morison's equation are used to deal with the hydrodynamics, while the aerodynamic forces are just reduced into a function of the relative wind speed. Nielsen et al. (2006) conducted integrated dynamic analysis for the Hywind concept and compared the results with scale experiments. In the above studies, the Morison's equation and/or potential thoery is used for hydrodynamics and BEM is used for aerodynamic forces. The empirical nature of Morison's equation may lead to limitation for new design shape of floating platforms and these can be seen in Roddier et al. (2010). Sebastian and Lackner (2013) shed light on the highly unsteady flow properties of floating wind turbines. Their study formulated that traditional BEM added with ad-hoc corrections cannot accurately model the interaction between the rotor and its wake. Other researchers like Nematbakhsh et al(2012) and Quallen et al (2013) made attempts to describe the interactions of waves on a FOWT using the full Navier-Stokes equations. In this

approach, the free surface motion is fully nonlinear and no empirical corrections are depended. It's worthy to note that Quallen et al. (2013) resolved the rotor geometry using overset grid technique. This work is a valuable attempt for fully CFD simulation of a floating wind turbine system, although this method is very time-consuming.

In the present study, in order to investigate the interaction of the aerodynamic loads with the platform motion within acceptable time cost, an unsteady aerodynamic code was developed and it was integrated with a two-phase fluid CFD solver, naoeFOAM-SJTU (Shen and Wan, 2012). The UALM, which is developed to model the unsteady aerodynamics of the rotor, will be detailed later. This model is capable of modelling the interaction between the rotor and its wake within acceptable accuracy and time cost. An embedded mooring-line module in naoeFOAM-SJTU is also developed to model the mooring dynamics.

NUMERICAL METHODS

In the present work, our focuses are on the motion responses and the fluctuating aerodynamic loads. In order to simulate the coupled dynamics, an unsteady actuator line model is developed and integrated with the fluid and motion solver, naoeFOAM-SJTU. We extend the original actuator line model presented by Sorensen and Shen (2002) to unsteady conditions by taking the effects of the platform motion into consideration.

Overall Governing Equations

The incompressible Reynolds-Averaged Navier-Stokes equations for both air and water used by naoeFOAM-SJTU as overall governing equations, can be written as:

$$\nabla \cdot \boldsymbol{U} = 0 \tag{1}$$

$$\frac{\partial \rho \boldsymbol{U}}{\partial t} + \nabla \cdot \left(\rho\left(\boldsymbol{U} - \boldsymbol{U}_g\right)\right)\boldsymbol{U} = -\nabla p_d - g \cdot \boldsymbol{x}\nabla\rho + \nabla \cdot \left(\mu_{eff}\nabla \boldsymbol{U}\right) + \left(\nabla \boldsymbol{U}\right) \cdot \nabla \mu_{eff} + \boldsymbol{f}_\sigma + \boldsymbol{f}_s + \boldsymbol{f}_\varepsilon \tag{2}$$

where $\boldsymbol{U}$ is the fluid velocity; $\boldsymbol{U}_g$ is velocity of mesh points, ρ is two phase mixture density; p_d is the dynamic pressure; g is the acceleration of gravity; $\mu_{eff} = \rho(\nu + \nu_t)$ is the efficient dynamic viscosity, in which ν and ν_t are the kinematic viscosity and the turbulence kinetic viscosity respectively; $\boldsymbol{f}_\sigma$ are the surface tension term in two phases model; $\boldsymbol{f}_s$ is the source term of the sponger layer for wave damping (Shen et al, 2012); $\boldsymbol{f}_\varepsilon$ is the volume forces of rotor blades which is projected back to the fluid field and detailed subsequently.

Unsteady Actuator Line Model

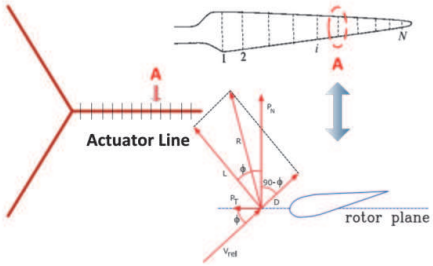

Fig. 1 Sketch of blade discretization

A fully resolved computational model including the full tower and the nacelle may be possible, but would surely be very demanding for computational resources. So an UALM was developed to model the rotor and its wake within acceptable time cost. The actuator line model (ALM) was an effective way to displace the real blade surfaces with virtual actuator lines (Troldborg, 2007 and Churchfield, 2012). In consequence, it acquire a benefit of not requiring to solve the blade geometry layer (Sorensen et al, 2002). This is accomplished by discretizing the blades into span-wise sections of constant airfoil, chord, twist and distributing the forces over them (Fig. 1). In this study, modifications are made to the initial ALM so that it can be used to simulate the FOWT. This is accomplished by accounting for the influence of the platform motion on the blades.

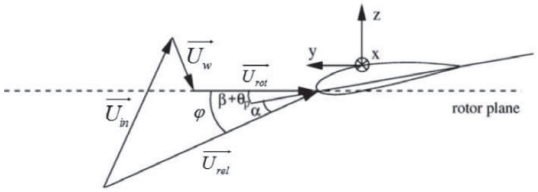

Fig. 2 Velocity triangle seen locally on a blade section

To find the relative velocity of an actuator point, $\boldsymbol{U}_{rel}$, the rotational velocity, $\boldsymbol{U}_{rot}$, plus the six DOFs motion velocity of the actuator point, $\boldsymbol{U}_w$, must be added as vectors to incoming wind velocity, $\mathbf{U}_{in}$, as shown in Fig 2. $\boldsymbol{U}_w$ is the additional velocity of the actuator point caused by the six DOFs motion of the floater. The relative velocity $\boldsymbol{U}_{rel}$ seen from the blade section and the flow angle φ with respect to rotor plane are determined as follows.

$$\boldsymbol{U}_{rel} = \boldsymbol{U}_{in} + \boldsymbol{U}_{rot} + \boldsymbol{U}_w \tag{3}$$

$$\varphi = \arctan\left(\frac{U_{rel,z}}{|\boldsymbol{U}_{rel}|}\right) \tag{4}$$

The first two terms in the formula of relative velocity is included in initial actuator line model. In order to simulate the rotor of floating wind turbine, we need to consider the additional velocity cause by the platform motion (e.g. $\boldsymbol{U}_w$). In Eq. 4, $U_{rel,z}$ is the velocity component of $\boldsymbol{U}_{rel}$ at the Z-axis .

To get the volume forces $\boldsymbol{f}_\varepsilon$, the blade element theory is used. The lift and drag force per span-wise length are calculated once the local angle of attack is given by $\alpha = \varphi - \gamma$, where γ denotes the local pitch angle.

$$\boldsymbol{f} = \frac{d\boldsymbol{F}}{rdrd\theta dz} = \frac{\rho U_{rel}^2 c N_b}{2rdrd\theta dz}\left(C_L\overrightarrow{e_L} + C_D\overrightarrow{e_D}\right) \tag{5}$$

Where C_L and C_D are two-dimensional airfoil lift and drag coefficients, which are determined by lookup table. In Eq. 5, r is the local radius, c is the local chord, N_b is the number of blades and $\overrightarrow{e_L}$, $\overrightarrow{e_D}$ are the directional vectors of lift and drag respectively. The applied aerodynamic blade forces need to be distributed smoothly on several mesh points in order to avoid singular behavior. In practice, a 3D Gaussian function is made to smooth the force over the blade by taking

the convolution of the force with a regularization kernel, $f_\varepsilon = f \otimes \eta_\varepsilon$, where

$$\eta_\varepsilon(d) = \frac{1}{\varepsilon^2 \pi^{3/2}} \exp\left[-\left(\frac{d}{\varepsilon}\right)^2\right] \tag{6}$$

Here, d is the distance between cell-centered grid points and the $i'th$ actuator line point, and ε is parameter that serves to adjust the concentration of the regularized loads.

Six DoFs Motion and Solving Strategy

The 6 DoFs motion solver embedded in naoeFOAM-SJTU adopted two coordinate systems: one is the earth-fixed coordinate system; the other is fixed on platform. The equations of motion are solved in platform-fixed system while the forces calculation are conducted in earth-fixed coordinate system. At every time step the transformation matrix **[*J*]** and velocity component of an actuator point cause by 6DoF motion U_w are updated using the following formula:

$$\boldsymbol{U}_{w,i} = [\boldsymbol{J}]\left(\boldsymbol{U}_c + \boldsymbol{\omega}_c \times (\boldsymbol{x}_i - \boldsymbol{x}_c)\right) \tag{7}$$

Where $\boldsymbol{U}_{w,i}$ is the additional velocity of the $i'th$ actuator line point in earth-fixed coordinate system; $\mathbf{U}_c$, $\boldsymbol{\omega}_c$, $\boldsymbol{x}_c$ are the velocity, angular velocity and coordinate of the rotating center respectively.

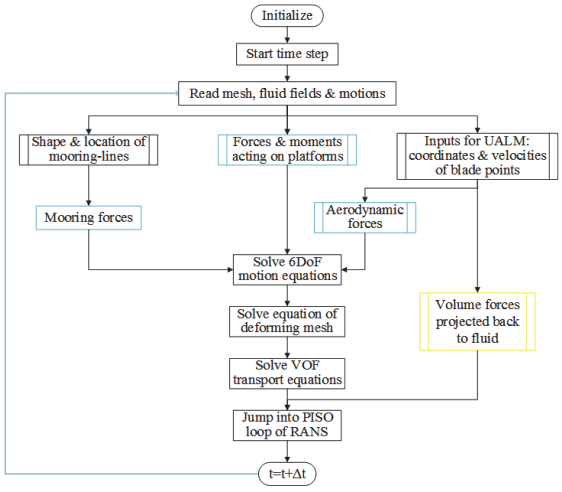

Fig. 3 Flow chart of solving strategy of coupled aero-hydro simulation

The complete solving process of the coupled dynamic simulation is shown in Fig 3. In practice, the Courant Number of the air flow is about one order of magnitude higher than that of the water flow. Therefore, we set up a parameter in the program to control the update frequency of the blade forces and volume forces. In other words, it could be useful to update the ALM calculation every 5 or 6 time steps. This practice may save the computational time. For the solving of the mooring forces, a quasi-static method, the Piecewise Extrapolating Method (PEM), is used. In contrast to catenary equation of lowest complexity, this method takes the effects of tension and the fluid forces into consideration. A more complex dynamic analysis method is also going to be accomplished in the near future.

The validation of UALM

Tran (2014) have conducted unsteady aerodynamic analysis of a floating offshore wind turbine experiencing platform pitching motion using Unsteady Blade Element Momentum theory (UBEM) and CFD. The business software star-CCM+ was used in his study. We have developed an Unsteady Actuator Line Model (UALM) to simulate the unsteady aerodynamics of the FOWT experiencing platform 6 DoFs motion. In order to validate this model, the same cases in Tran's paper are modelled here. The comparison of the three methods (UBEM, CFD, UALM) are shown in Fig 4 and Fig 5. A pitching platform motion of sine form (Eq. 9) is imposed on the floating platform. In Eq.9, θ_{pitch} is the pitch angle, Amp is the pitch amplitude and *Freq* is the pitch frequency. The rotating center of the pitching motion was assumed to be 90 m below the hub center in the z-direction.

$$\theta_{\text{pitch}} = \text{Amp} \cdot \sin(2\pi \cdot Freq \cdot t) \tag{9}$$

The comparison of unsteady aerodynamic power and thrust for platform pitching motion with amplitude=1°, frequency=0.1Hz is shown in Fig 4, while that with Amplitude=4°, frequency=0.1Hz is shown in Fig. 5. From these pictures, we can see the period of unsteady forces is approximately equal to twice times of the rotor rotation. The results in this paper using UALM are very close to the results of the other two methods used by Tran (2014). This proved that the unsteady actuator line model we've developed is correct. So we have confidence to use the UALM to calculate the unsteady aerodynamics of floating offshore wind turbine experiencing additional platform motion.

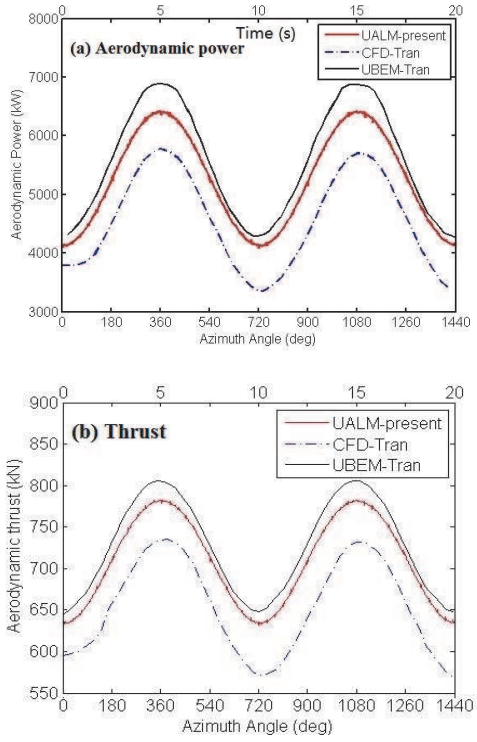

Fig. 4 The comparison of transient aerodynamic power and thrust for platform pitching motion with Amp=1°, *Freq*=0.1Hz

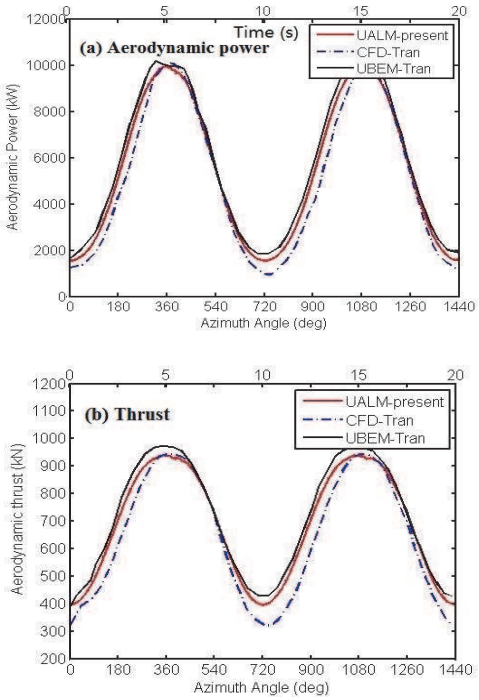

Fig. 5 The comparison of unsteady aerodynamic power and thrust for platform pitching motion with Amp=4°, *Freq*=0.1Hz

SIMULATION CONDITIONS

Description of the Computational Model

A specific DeepCwind floating wind system as shown below in Fig 6 is chosen in OC4 Phase II. The OC4-DeepCwind is mounted with the NREL's offshore 5MW baseline wind turbine (Jonkman et al, 2009). A three-bladed rotor is used , which located 90m above the SWL. The platform has a draft of 20m in the depth of 200m. The detailed floating platform geometry data can be found in Robertson et al. (2012).

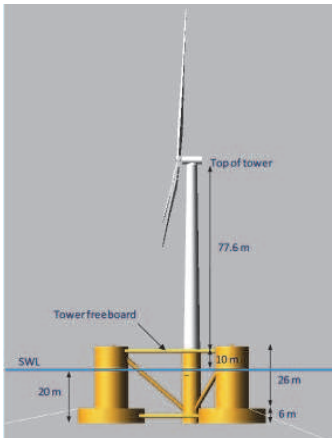

Fig. 6 DeepCwind floating wind system design

The motion responses cannot be computed accurately without accounting for the mass and the inertia of the tower and the nacelle, the wind forces and the forces from the mooring lines. In the present study, therefore, the nacelle, the tower and the platform are modelled as one mass of rigidity. The overall center of mass and moments of inertia are listed in Table 1. To secure the platform, the OC4-DeepCwind semisubmersible is moored with three catenary lines spread symmetrically about the central column of the platform. The mooring layout in the basin is shown in Fig 7. Detailed description of mooring system is provided in Robertson et al. (2012). The numbering of mooring lines is also shown in Fig. 7.

Table 1 Mass and inertial moment of OC4 DeepCwind

Platform mass including ballast, hub, nacelle and tower	1.402E+7 kg
Overall CM location excluding rotor& catenaries	(0.01228,0,-10.2604)
Overall roll inertia about CM	1.0776E+10 $kg \cdot m^2$
Overall pitch inertia about CM	1.0776E+10 $kg \cdot m^2$
Overall yaw inertia about CM	1.2265E+7 $kg \cdot m^2$

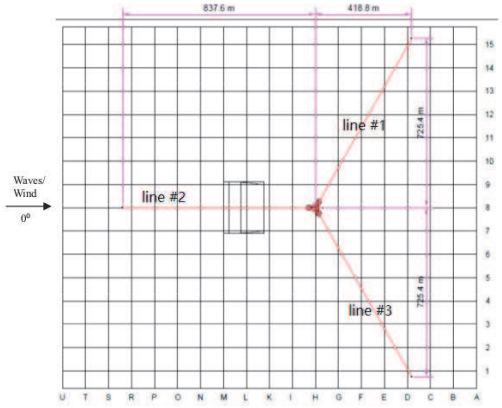

Fig. 7 Layout of mooring lines.

Wind and Wave Conditions

Two kind of full-system simulations with different complexity are performed: first, the wind forces are simplified into a constant thrust; second, the fully coupled dynamic analysis with wind and wave excitation is conducted by utilizing the UALM. In case A, the aerodynamic force acting on the platform is simplified to a constant thrust. The thrust is previously calculated by Actuator Line Model within only the wind excitation (The platform is assumed to be fixed.). Then we transform this thrust to the gravitational center of the platform and get a constant force （212kN）and a constant moment (2.13E4 $kN \cdot m$) as its equivalent forces. Case B introduces the wind and wave excitation so as to examine the system coupled responses with all DoFs enabled for the floater and the rotor. In case B, the rotor rotation is fixed at 7.45rpm and the platform operates in regular airy wave and steady wind. The wind and wave conditions are detailed in Table 2 and the wave condition is first defined by Robertson (2012). In fully coupled simulation case (case B), the unsteady actuator line model is used to calculate the aerodynamic forces and far wake flows within consideration of the wind shear of exponential law.

Table 2: A condition summary of simulation cases

case	Wind conditions	Wave conditions	Rotor	Output
A	NA	Regular airy: H = 3.66 m,T = 9.7 s	Locked	Platform response, mooring forces, water flow field
B	Steady, shear: V_{hub} = 5m/s	Regular airy: H = 3.66 m,T = 9.7 s	7.45rpm	aerodynamic forces, platform response, mooring forces, air & water flow field

Grid Topology

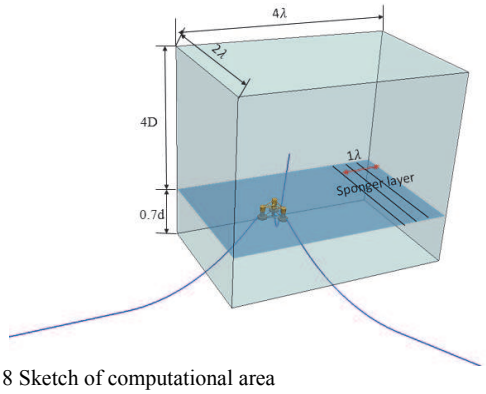

Fig. 8 Sketch of computational area

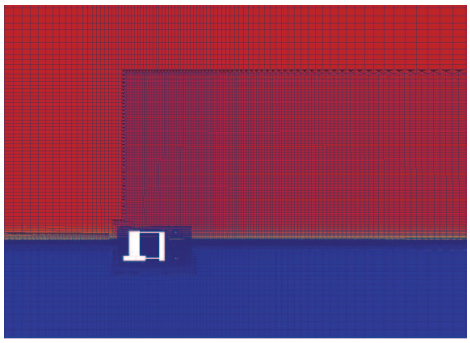

Fig. 9 A local slice of grid near platform

The computational domain used in case B is shown in Fig 8. In that Figure, λ means wave length. In case B, the wave-inlet boundary condition is set on the left side, while a sponge area with a length of about one wave-length is used behind to damping the wave. The computational domain is 4D (D is the rotor diameter) higher than the SWL and 0.7d (d is the water depth) lower than the SWL along the Z-direction. The computational domain in case A is a little different from case B. The computational domain specifically in case A is just 50 meters higher than the SWL along Z-direction because the field of air phase is not needed to be simulated. A partial slice of the grid is shown in Fig. 9. Local refinements are applied near the free surface, platform model and three radii downstream the rotor. The total number of grid cells for case B is 2.2 million.

RESULTS AND DISCUSSION

The unsteady actuator line model has been validated in section 2. In this section, the results of the cases described in Table 2 are presented and compared including the unsteady aerodynamic loads, platform motion responses, mooring-line forces and flow fields.

Unsteady Aerodynamic Loads

In case A, the aerodynamic forces are reduced to a constant thrust (212kN) and a moment of thrust acting on the gravitational center of the platform. In case B, the time history of aerodynamic power and thrust calculated by UALM are shown in Fig. 10 and Fig. 11 respectively. The total simulation time for two cases is 150 seconds.

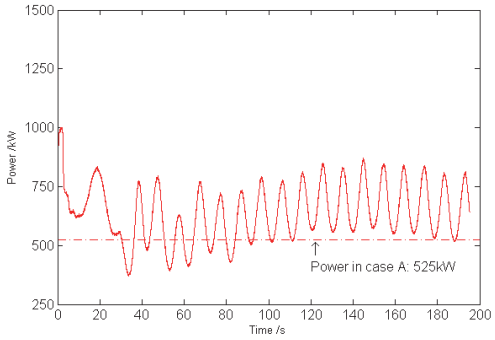

Fig. 10 The time history of transient aerodynamic power

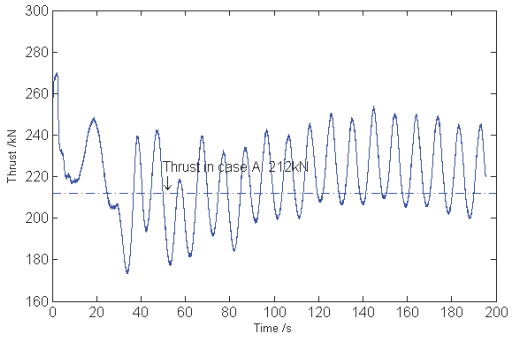

Fig. 11 Time history of transient aerodynamic thrust

We can see from the two figures that the aerodynamic thrust and power of the rotor fluctuate greatly due to the six DOFs motion of the floater. Specifically, the additional six Degrees of Freedom imposed on the floating foundations results in the highly unsteady properties of the floating wind turbine aerodynamics. So, the aerodynamic power and thrust are fluctuating significantly. Proper control strategy should be taken to ensure the stability of power output of the rotor in the case of the FOWT. The period of incident wave is 9.7s. About after 80s of simulation, the changing aerodynamic loads shows periodical property. The varying period is about 10 s, is approximately equal to the wave period. The thrust and aerodynamic power are all bigger than steady value (the dotted lines). The platform responses will be more significant because of the predicted bigger thrust in fully coupled case.

Platform Motion and Mooring-line Responses

The comparison of the platform response in case A and case B is shown in Fig 12. The red line corresponds to the motion responses of case B, while the other blue one to case A. In case A, the platform motion in surge, yaw and roll degree of freedom is seriously underestimated, while the pitch and heave response is a little overrated. The reason is that we don't take the coupling effects between the rotor aerodynamics and the floater's hydrodynamics into consideration in that simplified case. In case A, the predicted sway and roll motion is negligible while the predicted sway and roll motion is small but not negligible in case B. In the fully coupled case the predicted surge motion is much huger than that in case A. The predicted maximum of surge motion in case B is up to 15 meters. This significant surge motion leads to a violent interaction between the rotor and its wake and, therefore, this motion has a direct impact on the aerodynamic performance of the FOWT. It's also interesting that a surprising yaw motion with amplitude up to 2° is predicted in case B. This kind of significant yaw motion is totally unpredictable in the simplified case A. The torque exponent at the Z-axis exists in case B due to the cone angle of the rotor. So, in that case yaw motion is much more significant than case A.

To sum up, the unsteady aerodynamic loads have obvious effects on the platform motions. So the coupling effects between rotor aerodynamics and the floater's hydrodynamics is very important and cannot be negligible if we want to predict platform motion response with high accuracy.

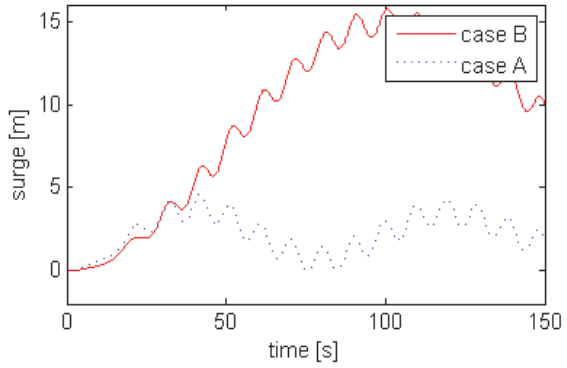

(a) surge

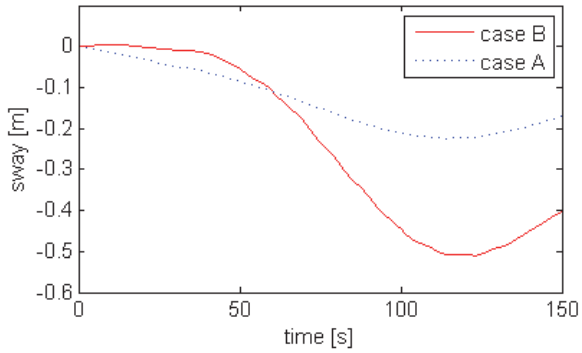

(b) sway

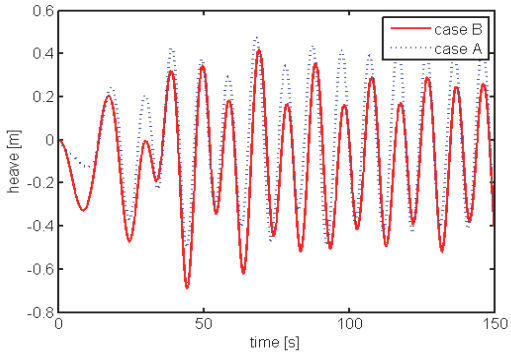

(c) heave

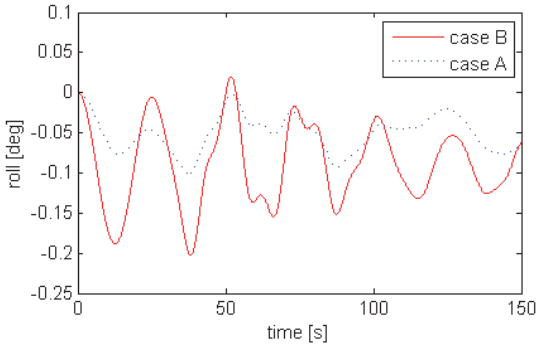

(d) roll

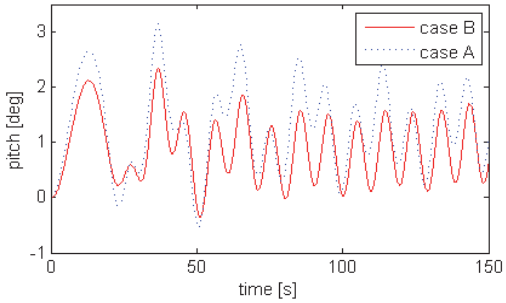

(e) pitch

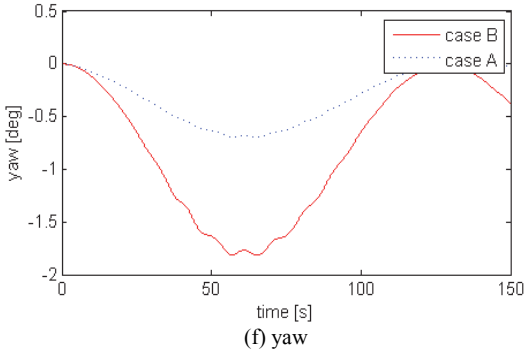

(f) yaw

Fig. 12 The comparison of platform motion responses

The comparison of the tension time history of mooring line #1 and mooring line #2 are shown in Fig. 13 and Fig. 14 respectively. The line #3 is placed symmetric to line #1 along wave direction. The tension of

line #3 is almost equal to line #1, so the time history of tension of line #3 is not presented here. We can see from Fig. 13 that the tension of line #1 of case A has larger values than those of case B. In Fig. 14, for line #2, the tension of case B is much bigger than that of case A. This phenomenon may be because of the large surge motion observed in the case of fully coupled dynamic simulation.

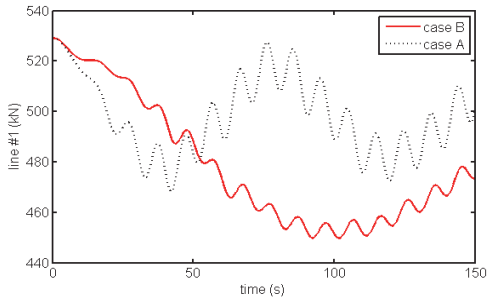

Fig.13 Comparison of tension history of mooring line#1

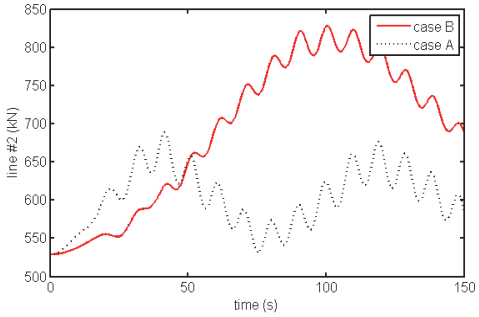

Fig. 14 Comparison of tension history of mooring line#2

Flow Field Analysis

The evolution of wake vortex at a representative cycle (namely 0T, 0.25T, 0.5T and 0.75T) for case B is illustrated in Fig 15(a)-(d). The wake vortex of the rotor as shown in Fig. 15 are visualized by the second-order invariant of velocity gradient, Q. In Fig. 15, the wave is contoured by wave height and the catenary is represented by three black lines. A clear and stable spiral vortex appears at the tip of rotor. The radius of the spiral-like wake expands when the wake develops downstream. The wake structure deform towards downstream due to the rotor moving into and out of its wake flows imposed by additional platform motion. The wake vortex quickly break towards downstream and then gather into new tip vortex.

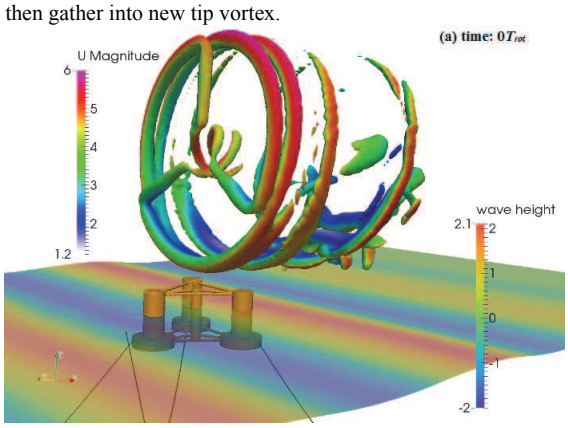

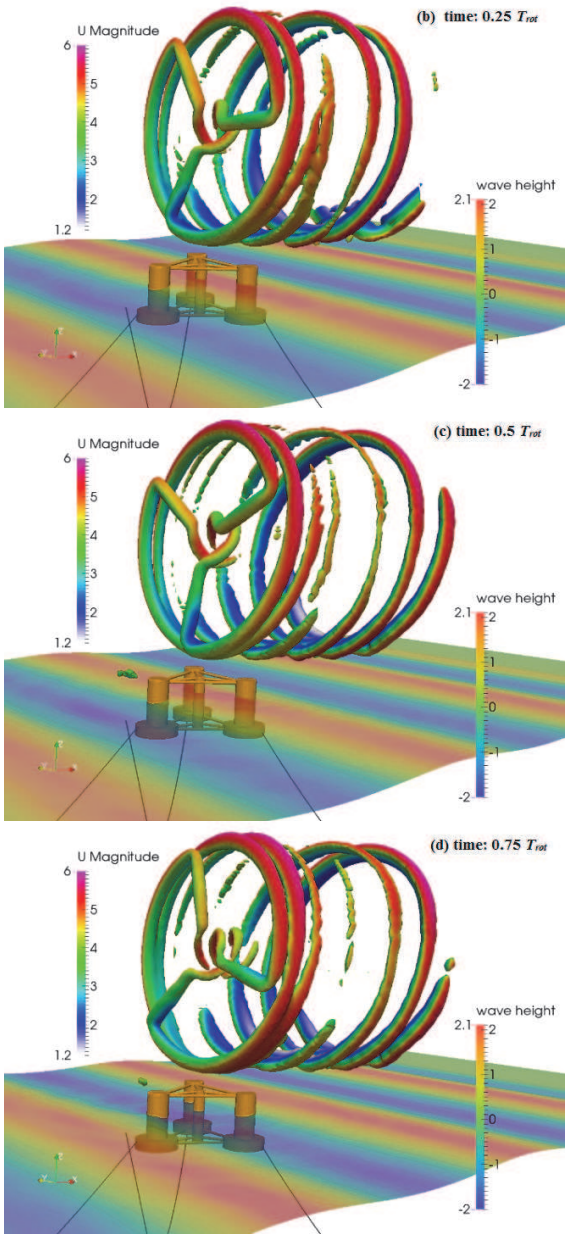

Fig. 15 Wake development of Rotor and wave height contour in case B.

Fig. 16 shows the dynamic pressure distribution of the floating platform in simplified case A at simulation time t = 192.6 s. In Fig. 16, grey color indicates the free surface while in Fig. 17 blue color indicates the free surface. Fig. 17 shows the dynamic pressure distribution of the floating platform in coupled simulation case B at simulation time t = 192.6 s. The maximum dynamic pressure on the floating platform is about 18000Pa in case A, but that in case B is more than 20000Pa. That means the coupled effects between the aerodynamic forces and the hydrodynamic forces have a significant influence over the pressure distribution on the platform surface. In case B, larger platform motion responses are predicted, so the damping pressure acting on the platform

by the moving wave is more significant.

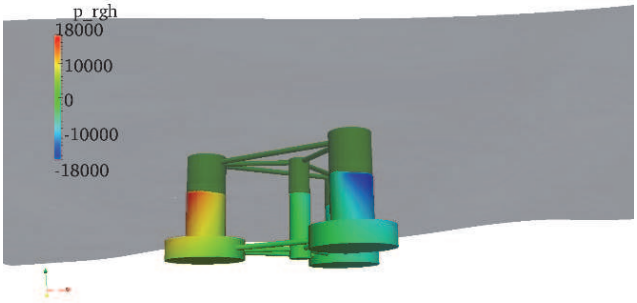

Fig. 16 Dynamic pressure distribution of floating platform（case A）

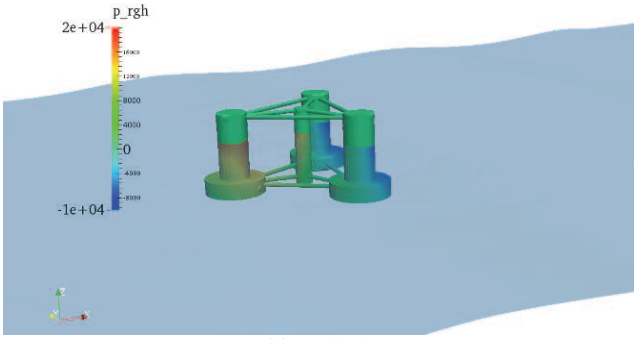

(c) t=192.6s

Fig. 17 Dynamic pressure distribution of floating platform（case B）

CONCLUSIONS

The combined aerodynamic, hydrodynamic, and mooring-system dynamic effects on FOWT create unique operating and failure design conditions which have not yet been studied in great detail. In the present study, in order to investigate the interaction of the aerodynamic loads with the platform motions including the mooring system within acceptable time cost, an unsteady aerodynamic code was developed and integrated with two-phase fluid CFD solver: naoeFOAM-SJTU. The UALM is validated first by comparing with previous study. The unsteady aerodynamic loads calculated by UALM agrees well with that calculated by UBEM and CFD.

Then the coupled dynamic analysis code was used to perform a rotor-floater fully coupled dynamic simulation. In order to investigate the importance of coupling effects, a simplified case is also studied. Two kind of full-system simulations with different complexity shows that the coupling effects is very important if we want to predict the aerodynamic loads and motion responses accurately. The platform responses show an influence from the changing aerodynamic loads, while the aerodynamic loads are significantly affected by the platform motion through wave-induced rotor dynamics. For the flow fields, the wake structure deforms towards downstream due to the interaction of the rotor with its wake flows. The coupling effects between the aerodynamic forces and hydrodynamic forces have a significant effect on the pressure distribution on the platform's surface. The maximum dynamic pressure on the floating platform's surface is much bigger because of the larger platform motion responses.

More work should be done to shed light on the coupled aero-hydro dynamic (including mooring system) effects. In the near future, we will perform more cases study for coupled dynamic simulation with different wind and wave conditions.

ACKNOWLEDGEMENTS

This work is supported by the National Natural Science Foundation of China (51379125, 51490675, 11432009, 51579145, 11272120), Chang Jiang Scholars Program (T2014099), Program for Professor of Special Appointment (Eastern Scholar) at Shanghai Institutions of Higher Learning (2013022), Innovative Special Project of Numerical Tank of Ministry of Industry and Information Technology of China (2016-23) and Foundation of State Ley Laboratory of Ocean Engineering (GKZD010065), to which the authors are most grateful.

REFERENCES

Cordle, A, Jonkman, J. M., and Hassan, G (2011). "State of the art in floating wind turbine design tools," *National Renewable Energy Laboratory.*

Jonkman, JM, Butterfield, S, Musial, W, and Scott, G (2009). "Definition of a 5-MW reference wind turbine for offshore system development," *Golden, CO: National Renewable Energy Laboratory.*

Karimirad, M, & Moan, T (2012). "A simplified method for coupled analysis of floating offshore wind turbines," Marine Structures, 27, 45–63.

Matha, D, Schlipf, M., Cordle, A, Pereira, R, and Jonkman, J (2011). "Challenges in simulation of aerodynamics, hydrodynamics, and mooring-line dynamics of floating offshore wind turbines," National Renewable Energy Laboratory, US Department of Energy, Office of Energy Efficiency and Renewable Energy.

Musial, W, Butterfield, S, & Boone, A (2004). "Feasibility of floating platform systems for wind turbines." *In 23rd ASME Wind Energy Symposium, Reno, NV.*

Nematbakhsh, A., Olinger, D. J, and Tryggvason, G (2012). A nonlinear computational model for floating wind turbines. In 5th Symposium on Transport Phenomena in Energy Conversion from Clean and Sustainable Resources, Rio Grande, PR.

Nielsen, F. G, Hanson, T. D, and Skaare, B (2006). Integrated dynamic analysis of floating offshore wind turbines. In 25th International Conference on Offshore Mechanics and Arctic Engineering (pp. 671–679). American Society of Mechanical Engineers.

Shen, Z and Wan, DC (2012). "Manual of CFD solver for ship and ocean engineering flows: naoe-FOAM-SJTU." Technical Report No. 2012SR118110, Shanghai Jiao Tong University.

Quallen, S., Xing, T., Carrica, P., Li, Y., Xu, J. et al. (2013). "CFD simulation of a floating offshore wind turbine system using a quasi-static crowfoot mooring-line model," In The Twenty-third International Offshore and Polar Engineering Conference. Anchorage, Alaska, ISOPE, 2.

Ramachandran, G, Bredmose, H, Srensen, J, & Jensen, J (2013). "Fully coupled three-dimensional dynamic response of a TLP floating wind turbine in waves and wind," *In Proceedings of the ASME 2012 31st International Conference on Ocean, Offshore and Arctic Engineering (pp. 299–308).* American Society of Mechanical Engineers volume 7.

Robertson, A, Jonkman, J., Masciola, M, Song, H., Goupee, A., Coulling, A., & Luan, C. (2012). Definition of the semisubmersible floating system for phase ii of oc4. Offshore Code Comparison Collaboration Continuation (OC4) for IEA Task , 30.

Roddier, D., Cermelli, C., Aubault, A, and Weinstein, A. (2010).

"Windfloat: A floating foundation for offshore wind turbines," *Journal of Renewable and Sustainable Energy*, 2, 033104.

Sebastian, T., & Lackner, M. (2013). "Characterization of the unsteady aero- dynamics of offshore floating wind turbines," *Wind Energy,* 16 , 339–352.

Troldborg, N, Sørensen, J. N, & Mikkelsen, R (2007). "Actuator line simulation of wake of wind turbine operating in turbulent inflow," *In Journal of Physics:* Conference Series (Vol. 75, No. 1, p. 012063). IOP Publishing.

Churchfield M J, Lee S, Moriarty P J, et al. (2012) "A large-eddy simulation of wind-plant aerodynamics," *AIAA paper,* 2012: 537.

Sorensen, J. N., & Shen, W. Z. (2002). "Numerical modeling of wind turbine wakes," *Journal of fluids engineering*, 124 , 393–399.

Tran, T, Kim, D, & Song, J (2014). Computational Fluid Dynamic Analysis of a Floating Offshore Wind Turbine Experiencing Platform Pitching Motion. Energies,7(8),5011-5026.

Vir´e, A (2012). "How to float a wind turbine," *Reviews in Environmental Science and Bio/Technology* , 11 , 223–226.